Research Article

For reprint orders, please contact: reprints@futuremedicine.com

Nanomedicine

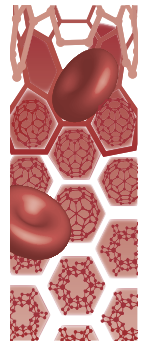

Distribution of polymer-coated gold nanoparticles in a 3D lung model and indication of apoptosis after repeated exposure

Savvina Chortarea[1,2], Kleanthis Fytianos[1,3,4], Laura Rodriguez-Lorenzo[1], Alke Petri-Fink[1,5] & Barbara Rothen-Rutishauser*,[1]

[1]BioNanomaterials, Adolphe Merkle Institute, University of Fribourg, Fribourg, Switzerland

[2]Laboratory for Particles – Biology Interactions, Empa, Swiss Federal Laboratories for Materials, Science & Technology, St Gallen, Switzerland

[3]Department of Pulmonary Medicine, University of Bern, Bern, Switzerland

[4]Department of Clinical Research, University of Bern, Bern, Switzerland

[5]Department of Chemistry, University of Fribourg, Fribourg, Switzerland

*Author for correspondence: Tel.: +41 26 300 9502; barbara.rothen@unifr.ch

Aim: The distribution and impact of aerosol-delivered gold nanoparticles (AuNPs) functionalized with a mixture of aminated-polyvinyl alcohol and amino-PEG ([polyvinyl alcohol/PEG]-NH_2) upon repeated administration onto a 3D lung model were explored. **Materials & methods:** AuNPs were aerosolized and uptake and epithelial translocation was assessed by inductively coupled plasma optical-emission spectroscopy, flow cytometry and electron microscopy. In addition, cytotoxicity, apoptosis and proinflammation were evaluated. **Results:** Repeated AuNP aerosolization resulted in NP accumulation in macrophages and epithelial cells. Dendritic cells demonstrated substantial NP internalization after single administration which was reduced in later time points. No cytotoxicity or proinflammation was observed but after 96 h significant apoptosis was induced by the polymer coating. **Conclusion:** These results indicate the importance of repeated exposures in addressing potential effects of NPs.

First draft submitted: 28 November 2017; Accepted for publication: 27 February 2018; Published online: 6 June 2018

Keywords: air–liquid interface • biodistribution • biomedical gold nanoparticles • hazard assessment • *in vitro* 3D lung system • short-term repeated aerosol exposure

The respiratory tract with its large epithelial surface area of around 140 m^2 and a dense network of antigen-presenting immune cells, that is, macrophages and dendritic cells [1–3], is a promising target for noninvasive aerosolized drug and vaccine delivery [4,5]. Indeed, the lung is an ideal organ for drug administration, as it allows fast action, lower drug metabolism and higher bioavailability of different-sized drug molecules for the treatment of respiratory, that is, asthma and systemic diseases, that is, diabetes [4,6]. Therefore, the inhalatory route offers several benefits over the classical oral or intravenous drug administration. In fact, pulmonary aerosol drug delivery has been successfully employed for several years for the therapy of lung diseases such as asthma, emphysema and chronic obstructive pulmonary disease [5]. Moreover, various potential respiratory drugs and vaccines are under development for the treatment and prevention of diabetes, cystic fibrosis, measles or even headache and pain relief [7]. However, despite these encouraging aspects, free antigen delivery directly to the pulmonary region often fails to induce pivotal protective reactions due to rapid degradation [8]. For this reason the design and development of novel drug carriers in the nanoscale is vital for the improvement of the performance of already existing as well as future drugs. Consequently, the potential of engineered nanomaterials in biomedical applications has gained significant scientific attention, over the recent years. In particular, engineered nanoparticles (NPs) are promising drug-carriers systems for site-specific deposition and targeted delivery in novel therapeutic applications [9,10]. Hence, an increasing number of aerosolized NP-based drug and vaccine carriers are under intense research investigation.

Future Medicine

NPs could provide new technological advances also in novel diagnostic approaches [11,12]. Depending on their size and physico-chemical properties inhaled NPs may interact with the lung epithelium, the first defense barrier and deposit either in the airway or the alveolar region. More specifically inhaled particles between 10 and 100 nm predominately deposit in the lower respiratory tract and in particular the lung parenchyma [13]. Therefore, great efforts have been made by both *in vitro* and *in vivo* approaches to discover the biological impact of inhaled NPs in the deep lung [14]. Moreover, NP interaction with the different lung cells types and the possibility to cross the ultra-thin air–blood barrier (which can be as thin as 0.1–0.2 μm [2]) and reach extra-pulmonary organs through the bloodstream are also crucial parameters that require investigation, before their employment in nanomedical applications [5].

Among the different types of engineered NPs, AuNPs hold particular promise in nanocarrier delivery systems and medical imaging, due to their high stability and tunability (i.e., shape, size, charge control), straightforward synthesis, high cell permeability, low apparent toxicity and their ability to target drug release (using appropriate surface modifications and addition of ligands) [15,16].

Recently, a library of fully characterized homo- and hetero-functional fluorescence-encoded biomedical AuNPs was established in our group using different polyvinyl alcohol (PVA) and PEG surface polymer probes for particle coating and stabilization [17]. Using this NP library, Fytianos *et al.* demonstrated that different surface modifications can greatly modify the interaction of AuNPs with monocyte-derived dendritic cells (MDDCs) as well the cell viability and proinflammatory response, while not affecting the immunological cellular properties, following 16-h submerged exposure [18].

The potential use of modified AuNPs as carriers of inhalative drugs or vaccines requires a better understanding of their interaction with lung cells and in particular with cells of the alveolar lung region and clear assessment of possible adverse effects that might occur upon single or repeated treatment. In fact, investigation of the distribution and biological response after repeated AuNP inhalation is of importance as drugs may have to be received repeatedly for an efficient disease treatment. Despite, the increasing literature proposing AuNPs for novel biomedical applications only limited knowledge is available regarding the effect of repeated inhalation in both *in vitro* and *in vivo* settings [19]. More specifically, *in vitro* studies have been mainly performed under submerged conditions and within relatively short incubation times (24–48 h). In the present study, the utilization of the air–liquid interface cell exposure system (ALICE), which realistically mimics *in vitro* the physiological conditions of aerosol inhalation in the lungs [20] together with an advanced 3D model of the human lung epithelial tissue barrier [21], offered an efficient platform to study the short-term repeated NP aerosol at air–liquid interface (ALI) conditions as described for carbon-nanotubes aerosols [22]. Our aim was to explore the distribution and the biological impact of aerosol-delivered biomedical AuNPs (fluorescently labeled and surface modified with a positively charged mixture of aminated PVA and PEG polymers ([PVA/PEG]-NH_2), on a sophisticated *in vitro* lung co-culture, upon a realistic short-term (up to 96 h) repeated scenario.

Materials & methods

Chemicals & reagents

All chemicals and reagents used were obtained from Sigma-Aldrich (Buchs, Switzerland), unless otherwise stated.

Synthesis & characterization of fluorescence-encoded hetero-(PVA/PEG)-NH2 AuNPs

Synthesis

Carbodiimide chemistry was used to conjugate the primary amines of vinylalcoho-vinylamine copolymer (PVA-NH_2; MW = 240,000 g/mol, Erkol S.A, Spain) and thiolated poly(ethylenglycol) amine (SH-PEG-NH_2; MW = 5000 g/mol, Creative PEG-Works, NC, USA) with the activated carboxyl groups of the ATTO590 NHS ester (Sigma-Aldrich) as previously described in Rodriguez-Lorenzo *et al.* [17]. AuNPs (15 nm in diameter, [Au] = 0.5 mM) were synthesized following the Turkevich procedure [23]. In order to prepare the (PVA/PEG)-NH_2 AuNPs, phosphate-buffered solution (PBS; pH 7.4) containing 12 mg of dye-conjugated polymer mixture calculated to provide a ratio of weight PEG:PVA 1:1 (mg) was prepared and sonicated for 20 min. Then, the polymer solution was added drop wise at room temperature under shaking to AuNPs suspension (20 ml) at weight ratio PEG:PVA:Au of 3:3:1 (mg). The mixture was incubated to reach the thermodynamic equilibrium at room temperature for 24 h under dark conditions. Labeled polymer-coated NPs were centrifuged (10000 ×*g*, 1 h) to remove excess polymer and redispersed in 20 ml of 1 × PBS. A second coating with unlabeled PEG/PVA mixture was then further applied

using same conditions. The final (PVA/PEG) – NH_2 AuNPs were centrifuged at 10,000 ×*g* for 1 h and redispersed in PBS.

Characterization methods

UV-visible (UV-Vis) spectra of the samples were recorded at 25°C using a Jasco V-670 spectrophotometer (Jasco Europe S.R.L., Milano, Italy), using 10 mm path length quartz cuvettes. The hydrodynamic radius of the AuNPs was measured at a concentration of 50 µg/ml in 1 mM PBS at 25°C by dynamic light scattering (DLS) at 90° using a commercial goniometer instrument (3D LS Spectrometer, LS Instruments AG, Fribourg, Switzerland). The surface charge of AuNPs samples was measured in suspension of 50 µg/ml in 1 mM PBS at 25°C using a phase amplitude light scattering ζ-potential analyzer (Brookhaven ZetaPALS, Brookhaven Instruments Corporation, NY, USA). The Smoluchowski approximation was fitted to 20 cycles of electrophoretic mobility measurements and ten replicates were obtained for each sample to estimate the mean and the standard deviation. The average number of ATTO590 molecules on the AuNPs was determined by using a PerkinElmer Victor Fluorescence Microplate Reader with 560/615 filter set (Wallac 1420 VICTOR3 reader, PerkinElmer, MA, USA). Then, 10 µl of AuNPs samples were dissolved with 10 µl of 40 mM KCN (Sigma-Aldrich) to avoid any interference during the fluorescence measurements. All measurements were carried out in triplicate.

Endotoxin content

The endotoxin concentration in AuNP suspensions was measured using the Pierce™ LAL Chromogenic Endotoxin Quantitation kit (Thermo Fisher Scientific, MA, USA), following the manufacturer's instructions.

Lung cell cultures

Exposure experiments were performed, using a sophisticated *in vitro* co-culture model of the human lung epithelial tissue barrier [21]. Briefly, the co-culture composed of a monolayer of A549 human (alveolar type II; American Type Culture Collection, Middlesex, UK) epithelial cells, combined with human blood monocyte-derived macrophages (MDMs) added on top of the epithelium and MDDCs, added underneath the membrane. A549 cells were maintained in Rosewell Park Memorial Institute (RPMI) 1640 medium, supplemented with 1% L-glutamine (L-Glut; Life Technologies [MA, USA]/Thermo Fisher Scientific), 1% penicillin/streptomycin (10,000 units/ml/10,000 µg/ml; Gibco [MA, USA]/Thermo Fisher Scientific) and 10% fetal calf serum (PAA Laboratories, Chemie Brunschwig AG, Basel, Switzerland), at 37°C, 5% CO_2. Cells were seeded at a density of 0.5 × 10^6 cells/ml, in BD Falcon™ cell culture inserts for six-well plates (transparent PET membrane, 3 µm diameter pore size and surface area of 4.2 cm^2; BD Biosciences, Allschwil, Switzerland). Inserts were placed in 6-well culture plates (BD Biosciences) and epithelial cells were grown under submerged conditions (2 ml medium in the apical and 3 ml in the basolateral side of the insert) for 5 days. In parallel, peripheral human blood monocytes were isolated from human blood buffy coats (Blood Donation Service, Bern University Hospital, Bern, Switzerland), as described by Blank *et al.* [24] and cultured for 6 days in supplemented RPMI medium. For the differentiation of MDDCs the growth factors GM-CSF and IL-4 (10 ng/ml) were added to the culture medium, whereas MDMs were obtained with the addition of MCSF (10 ng/ml).

The triple co-cultures were achieved, as previously described by Blank *et al.* (2007), resulting in a cell density of approximately 9714 epithelial cells/mm^2, approximately 231 MDM/mm^2 and approximately 411 MDDC/mm^2 [25]. After 24 h under submerged conditions, the co-cultures were transferred to the ALI, for additional 24 h, prior the exposures, by completely removing the medium in the apical chamber of the insert and by replacing the medium in the lower compartment with 1.2 ml of fresh medium.

Air–liquid interface cell exposure system

AuNPs were aerosolized using the ALICE system as described by Brandenberger *et al.* [26] and Fytianos *et al.* [27]. Briefly, the instrument consists of a nebulizer, an exposure and an incubation chamber connected to an air-flow system to provide optimum conditions for cell cultivation (RH: 80–95% and T: 37°C) as well as a quartz crystal microbalance (QCM) (operated at 5 MHz, lower detection limit: 0.09 µg/cm^2; Stanford Research Systems, Renens, Switzerland) for online measurements of the NP dose deposited on the cells surface. For each aerosolization, 1 ml of AuNP suspension (at the working concentration of 120 µg/ml) with 0.9% NaCl (NAAPREP® physiological saline, GlaxoSmithKline, Paris, France) was added to the nebulizer (eFlow nebulizer system, PARI Pharma GmbH, Starnberg, Germany). The vibrating perforated membrane of the nebulizer then generates the aerosol, which is

transferred into the exposure chamber where the cells are located. Inside this compartment, it gently deposits the aerosolized AuNP suspension onto cell cultures maintained at the ALI. The selected flow rate (5 l/min) is optimal for the aerosol to get sufficiently mixed to all sides of the chamber, thus resulting in uniform single droplet deposition.

Exposure scenario

To assess the biological impact and uptake efficiency of AuNPs upon short-term repeated aerosol exposures into the 3D *in vitro* lung model of the human epithelial tissue barrier, triple cell co-cultures were exposed repeatedly to (PVA/PEG)-NH_2 AuNPs (120 μg/ml) using the ALICE system. Cultures were transferred to ALI conditions at 0-h time point and exposures were performed at 24 h (first aerosolization), 48 h (second aerosolization) and 72-h time point (third administration) (Supplementary Figure 1). The cellular response was determined after a post-incubation time of 24 h following each AuNP exposure. Thus, sample collection occurred at 48-, 72- and 96-h time points. Cell cultures exposed repeatedly to dH_2O containing 0.9% NaCl were used as negative control.

Characterization of AuNP deposition after the aerosolization

Transmission electron microscopy

In order to characterize the deposited AuNPs aerosols, transmission electron microscopy (TEM) copper grids were exposed to aerosolized particles using the ALICE system. Representative images of the deposited AuNPs were captured using a TEM (Fei Technai Spirit; OR, USA), operating at 120 kV, fitted with a Veleta CCD camera (Olympus, Japan).

Quartz crystal microbalance

The deposition of aerosolized AuNPs was quantified by the incorporated QCM. In brief, the precise (PVA/PEG)-NH_2 AuNPs concentration deposited directly on the cells surface was determined by the linear decrease in the resonance frequency of the vibrating piezoelectric crystal, due to the increasing deposited mass. The differences in the frequency of the crystal, prior to and after aerosolization process were recorded and subsequently calculated to determine the mass per surface area (μg/cm^2), as previously described [20]. The deposition of aerosolized dH_2O containing 0.9% NaCl (negative control) was below the instruments detection limit.

Interaction of AuNPs with the human epithelial tissue barrier model

Inductively coupled plasma atomic emission spectroscopy (ICP-OES)

Sample preparation of ICP-OES

Following each post-incubation time, the cells and the basolateral medium of three different inserts were collected for ICP-OES analysis. More specifically, after the supernatant collection, cell de-attachment was achieved by apical and basolateral treatment with 500 μl of Trypsin-EDTA for 5 min. The cell suspension and the collected medium were then stored at -20°C until further analysis to quantify the distribution of Au in the system.

At 24 h before the measurements, samples were heated at 80°C and treated with 500 μl HNO_3 for 2 h. Then, 500 μl of aqua regia (HCl:HNO_3 = 3:1 volume ratio) were added and samples left overnight under the fume hood to completely digest the organic material and dissolve the AuNPs. The digested samples were transferred to 15 ml falcon tubes and diluted to 5 ml with water.

ICP-OES analysis

The treated samples were measured by ICP-OES (PerkinElmer Optimal 7000 DV, PerkinElmer, Schwerzenbach, Switzerland). Measurements were performed at a wavelength of 242.795 nm (limit of detection = 16 μg/l and limit of quantification = 23 μg/l), at an axial plasma view. The plasma flow was 15 ml/min and the sample flow rate 1.5 ml/min. A washing step was performed between each measurement and each sample was measured three-times. A standard curve of acidic aqueous Au solutions was recorded to quantify the amount of intracellular Au. Precision was defined by the coefficient of variation (CV% = [standard deviation/mean]*100), which was ≤10% for all the AuNP association studied. The accuracy was estimated by measuring the cellular uptake, the washing step (culture wash with PBS) and the AuNPs remaining in the cell culture media. The sum of these values was compared with the initial Au concentration. The recoveries were 100–120%. The spike recovery was estimated by spiking a known AuNP concentration in water and subjected then to the acid digestion and measured by ICP-OES. Average recoveries ranged from 99 to 103%.

Flow cytometry

The interaction of aerosolized AuNPs within the individual cell types, that is, epithelial cells, MDM and MDDC, and at the different tested time points was investigated as described previously by [27] and [28]. Briefly, at each time point, inserts were treated for 2 min with trypsin-EDTA (0.5 ml in the apical and 1 ml in the basolateral compartment). Then, the activity of trypsin was inhibited by the addition of 100 µl of FBS in each part. Subsequently, cells were washed with PBS and collected in flow cytometry tubes at a density of 10^6 cells/ml. Cell suspensions were stained with epithelial cell adhesion molecule EpCAM-APC (epithelial cell surface marker), CD80-FITC, CD40-Pacific Blue (both MDDC markers) and CD11a-PE-Cy7 (MDM surface marker) (dilution 1:50, all antibodies were purchased from Biolegend, CA, USA) at 4°C for 30 min. Flow cytometry analysis was performed with an LSR Fortessa instrument (BD Biosciences). For every measurement, 30,000 gated events were recorded. Gating and data analysis was performed with the FlowJo software (Tree Star, OR, USA) as described in [27].

Transmission electron microscopy

The cellular internalization of AuNPs following short-term repeated exposures at 48, 72 and 96 h was also investigated by TEM (Fei Technai Spirit) operated at 120 kV. Prior to the TEM analysis, sample preparation was performed as described by [26]. Briefly, exposed cultures were fixed with 2.5% glutaraldehyde in HEPES buffer, and then post fixed with 1% osmium tetroxide and stained with 0.5% uranyl acetate. Subsequently, the membranes were dehydrated in a graded ethanol series and embedded in Epon. Embedded cultures were cut in ultra-thin sections (50–80 nm), mounted on copper grids and stained with lead citrate and uranyl acetate. Images were captured with a Veleta CCD camera.

Biochemical analysis

Cytotoxicity

The release of LDH in the medium, a well-known indicator of membrane damage, was assessed using the commercially available LDH detection kit (Roche Applied Science, Mannheim, Germany), following the supplier's protocol. Each sample was tested in triplicate and LDH values were expressed relative to the negative control. The enzyme activity was determined photometrically, by measuring the absorbance at 490 nm (reference wavelength at 630 nm). Co-cultures exposed apically to 0.2% Triton X-100 for 24 h were used as positive control.

Apoptosis

Caspase 3/7 activation assay

The activation of caspase 3 and 7 in the repeatedly exposed cell cultures was quantified using the CellEvent Caspase-3/7 Green Flow Cytometry Assay Kit (Molecular Probes, Life Technologies) following the manufacturer's protocol. For the flow cytometry analysis 10,000 gated events were recorded, using the BD-LSR Fortessa. The gating strategy is displayed in Supplementary Figure 2. Co-cultures exposed to aerosolized (PVA/PEG)-NH_2 polymer only (40 µg/ml) were also assessed in order to investigate the impact of the surface modification in the observed apoptotic activity.

Annexin V assay

Early and late stages of apoptosis in AuNP-exposed cultures at 96 h were measured with the Annexin V Fluos kit (Roche Diagnostics, Zug, Switzerland) following the supplier's instructions. Flow cytometry analysis (10,000 gated events) was performed in the BD-LSR Fortessa and data were analyzed using FlowJo software (Tree Star). The gating strategy is shown in Supplementary Figure 2. Co-cultures (digested from the insert membrane) treated with camptothecin (2 µm; Sigma-Aldrich) for 30 min were used as positive apoptotic controls.

Proinflammatory response

IL-1β, TNF-α and IL-8 release were evaluated using the commercially available DuoSet ELISA Development Kit (R&D Systems, Switzerland), according to manufacturer's protocol. Triple cell co-cultures treated apically with 1 µg/ml of lipopolysaccharide (from *Pseudomonas aeruginosa*; Sigma-Aldrich) for 24 h served as a positive proinflammatory assay control.

Epithelial membrane integrity tests & cell morphology

Permeability Dextran Blue assay

Following the different tested time points (48, 72 and 96 h) the medium in the basolateral side of the cultures was replaced with 1 ml of supplemented RPMI medium (without phenol-red; Gibco). At the apical side 250 µl of phenol-free medium and 250 µl of 1% Blue Dextran (in PBS; GE Healthcare, Dietikon, Switzerland) were added. Cell cultures were then incubated for 2 h at 37°C in 5% CO_2 humidified atmosphere. Following the recommended incubation time the translocation of Dextran Blue in basolateral medium was quantified by measuring the absorbance at 600 nm. Cell cultures treated apically with 20 mM EDTA in phenol-free RPMI were used as positive control, as EDTA exposure results in the detachment of cells from the insert membrane [29]. Data were normalized to the translocation of Dextran Blue in an empty cell-free insert.

Laser scanning microscope

After the respective post-incubation periods, co-cultures were fixed for 15 min in 4% paraformaldehyde in PBS and stored at 4°C in PBS until further usage. To remove remaining paraformaldehyde cells were treated with 0.1 M glycine for 15 min and subsequently permeabilized in 0.2% Triton X-100 in PBS, for another 15 min. Samples were stained with phalloidin rhodamine (R-415; Molecular Probes, Life Technologies Europe B.V., Zug, Switzerland; dilution 1:50) and DAPI (Sigma-Aldrich; dilution 1:50) for F-actin cytoskeleton and nucleus, respectively. For optical analysis, samples were embedded in Glycergel (DAKO Schweiz AG, Baar, Switzerland). Sample visualization was performed using an inverted laser scanning confocal microscope 710 (Axio Observer.Z1, Carl Zeiss, Germany). Image processing was achieved using the restoration software IMARIS (Bitplane AG, Zurich, Switzerland).

Statistical analysis

For each data point three independent experiments were performed and data are presented as the mean ± standard error of the mean. Statistical analysis was performed using GraphPad Prism 5 (GraphPad Software Inc., CA, USA). A parametric one-way analysis of variance followed by Bonferroni *post hoc* test was performed. Results were considered significant if $p < 0.05$.

Results

AuNPs synthesis & characterization before aerosolization

The monodispersed and citrate-stabilized AuNP core (average TEM diameter 15 nm) was synthesized following the Turkevich approach [23]. A representative TEM image of the citrate AuNPs is shown in Figure 1A. AuNPs were coated with a mixture of PVA and PEG polymers with positive ($-NH_3^+$) charge and were tagged to ATTO590 fluorescent molecules as recently described by Rodriguez-Lorenzo *et al.* [17]. To avoid possible effect of fluorophore on the cellular uptake, the Au core was initially coated with a dye-conjugated mixture of amine-PVA and PEG, followed by the addition of the analogous unlabeled polymer mix (Figure 1). Before applying the particles in cell aerosolization experiments, AuNPs were thoroughly characterized in terms of colloidal stability using UV-Vis, hydrodynamic radius and polydispersity index using DLS, and surface charge through ζ-potential measurements of NP suspensions in PBS. No signs of aggregation, that is, red shifting or band broadening, were observed in the UV-Vis spectrum, confirming the stability of the employed AuNP suspension (Figure 1B). DLS analysis revealed an average hydrodynamic diameter of 58 nm with 12% polydispersity index and a ζ-potential of -6.1 ± 2 mV (Figure 1C). The slightly negative ζ-potential may be explained by the reduced number of protonated amino groups (1.5–2 fold) at pH 7 as well as by the remaining citrate molecules on Au surface (citrate AuNPs showed negative ζ-potential: -28 mV) [17,30]. Furthermore, quantification of the number of dye molecules in (PVA/PEG)-NH_2 AuNPs showed an average of 600 ± 10 fluorophore molecules per particle. Endotoxin levels were below 0.1 endotoxin unit/ml.

AuNP characterization after aerosolization

The ALICE is an efficient and well-established system for the aerosolization of spherical NPs [14,20,27,31,32] that recently proved effective to investigate possible effects in lung cells *in vitro* after short- and long-term repeated exposures to fibrous nanomaterials [22,33]. For each exposure, 120 µg/ml of AuNPs suspension was aerosolized using the ALICE system. Visualization of the deposited AuNPs on TEM grids following single and repeated aerosolization by TEM revealed a reproducible, homogeneous and dose-dependent particle deposition, while the particles remain monodispersed (Figure 2C & D). In addition, the deposited AuNP dose was determined online

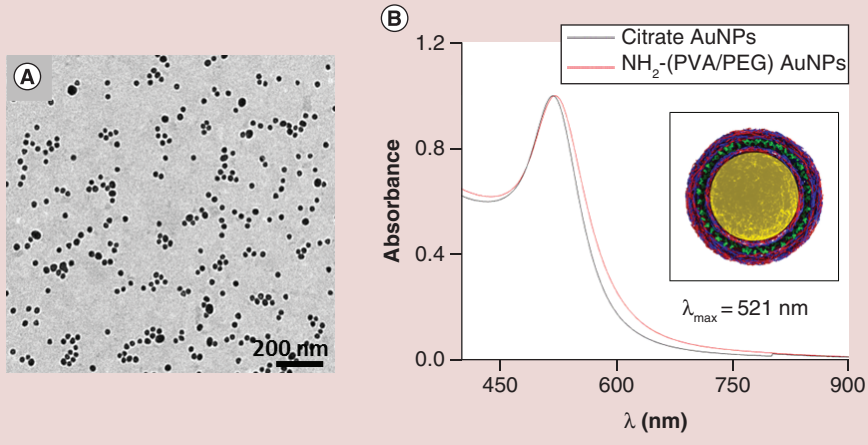

C

Hetero-functionalized AuNPs	Hydrodynamic diameter [nm] (polydispersity)	Zeta potential [mv] (SD)	Fluorophore molecules per AuNP (± SD)
NH_2-(PVA/PEG)	58 (12%)	-6.1 (2.0)	600 (± 10)

Figure 1. Characterization of Au nanoparticles suspension. (A) Transmission electron microscopy image of 15 nm AuNPs core. **(B)** UV-visible spectra of the citrate and ATTO590 NH_2-(polyvinyl alcohol/PEG) AuNPs. Inset: Schematic design of the heterofunctionalized AuNPs. **(C)** Physico-chemical characteristics of the AuNPs.
NP: Nanoparticle; SD: Standard deviation.

by the integrated QCM at the different tested time points. As shown at Figure 2E, the deposited NP mass (AuNPs mass and PVA/PEG mass) following single exposure was 7.24 ± 0.66 μg/cm^2 while the deposited mass upon two and three repeated aerosolization was 15.37 ± 1.27 and 23.24 ± 1.86 μg/cm^2, respectively. As expected the total Au content applied to cells was much lower 0.51 ± 0.07 (single exposure). No change was observed in the UV-Vis spectra of aerosolized AuNPs compared with their spectrum before the aerosol exposure while their hydrodynamic diameter (55 nm) was similar to the diameter of the stock suspension, indicating that the aerosolization process did not affect neither the colloidal stability nor the polymer surface coating of the AuNPs.

Interaction of AuNPs with the human lung epithelial tissue barrier model

The distribution of AuNP was investigated regarding their cellular uptake and translocation at different time points, that is, 24, 48 and 72 h, by measuring the mass of Au by ICP-OES in the individual compartments (i.e., cellular fraction and in the basal medium). As shown by Figure 3A, AuNPs displayed a concentration-dependent increase in the cellular fraction upon short-term repeated administration. In particular, single NP aerosolization (48 h) resulted in 26.9% AuNP attached and/or in the cells which was elevated after the second AuNP exposure (36.6%; 72 h). Notably, a significant increase in interaction was observed after the third repeated AuNP administration (43.1%; 96 h). The translocation of AuNPs across the human lung epithelial tissue barrier was also investigated. Interestingly, a high translocation rate was measured upon single dose exposure at 48 h, while a significant decrease in particles translocated in the basal medium was observed after repeated AuNP aerosolization at both 72 and 96 h time points.

For a more detailed investigation about the interaction of AuNPs with the different cell types of the *in vitro* co-culture system a flow cytometry approach was used which can detect the fluorophore incorporated in the polymer shell. Cells were labeled with specific cell surface markers for multicolor flow cytometry detection as recently described by [27,28]. AuNP uptake was determined as the frequency (percentage) of ATTO590 positive cells from the CD11a$^+$ (MDMs), EpCAM+ (epithelial cells) and CD80$^+$ (MDDCs) cell populations. In accordance with the ICP-OES findings, high particle cellular uptake was observed at all tested time points. AuNPs were found interacting

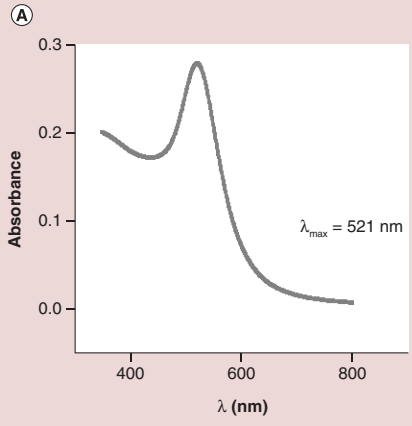

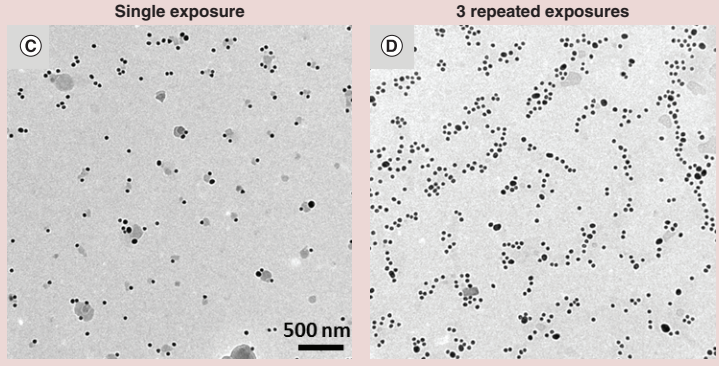

B

Hetero-functional AuNPs	Hydrodynamic diameter [nm]
NH_2-(PVA/PEG)	54.56

E

NH_2-(PVA/PEG) AuNPs	1st exposure	2nd exposure	3rd exposure
Total deposited mass [μg/cm²] (±SD) (QCM measurement)	7.24 (±0.66)	15.37 (±1.27)	23.24 (±1.86)
Total deposited Au [μg/cm²] (±SD) (ICP measurement)	0.51 (±0.07)	0.84 (±0.11)	0.94 (±0.04)

Figure 2. Characterization of aerosolized Au nanoparticles. (A) UV-visible spectra of the aerosolized ATTO590 NH_2-(polyvinyl alcohol/PEG)AuNPs using air–liquid interface cell exposure system system. **(B)** Hydrodynamic diameter of the aerosolized AuNPs. **(C)** Transmission electron microscopy images of deposited AuNPs following single or **(D)** three repeated aerosolization (scale bar for both images: 500 nm). Total deposition (mass per surface area) of aerosolized AuNPs upon single or repeated administration as measured by the quartz crystal microbalance and the inductively coupled plasma spectroscopy.
ICP: Inductively coupled plasma; NP: Nanoparticle; QCM: Quartz crystal microbalance.

with all the three cell types of the *in vitro* model (Figure 3B). Following single AuNP aerosolization (48 h), MDMs showed the highest frequency of particle-positive cells (54.5%) compared with epithelial cells (13.9%) and MDDCs (49.8%). Although the MDM-positive cells were significantly decreased (20.4% at 72 h and 24.5% at 96 h time point) after repeated administration, NP uptake still remained in substantial levels in MDMs upon the short-term exposure period. Low NP interaction was reported upon single NP exposure in epithelial cells, subsequently followed by a significant increase at 72 and 96 h time point (40.8 and 53%, respectively). Interestingly, approximately 50% of the MDDC population was ATTO590 positive, after one aerosolization, which could potentially explain the enhanced translocation observed at this time point. Repeated AuNP administration resulted in a significant decrease in MDDC-positive cells (20.2% at 72 h and 15.6% at 96 h). Notably, the MDDC NP uptake follows a similar pattern with the AuNP translocation data which were similarly decreased at the latter time points.

The internalization of AuNPs by the cells was qualitatively confirmed by TEM. Indeed, internalized AuNPs were visualized in all the three cell types of the co-culture model and at all tested time points (48, 72 and 96 h) as shown by the TEM images in Figure 3C and Supplementary Figure 3, hence further supporting the flow cytometry findings. NPs are mainly present either as single particles or as small agglomerates (of few particles) mostly inside intracellular vesicles. Of great interest is the observation of particles inside cellular protrusion in the membrane pores of the insert, possibly captured while translocating from the apical to the basolateral compartment through cell to cell interaction (Supplementary Figure 4). Moreover, several particles in the apical side were located close to the membrane of the insert (data not shown), indicating a possible relocation to the basolateral side which could explain the substantial uptake found in MDDCs by flow cytometry. Of note, internalized AuNPs were often observed in cellular protrusions of MDDCs (Supplementary Figure 4C).

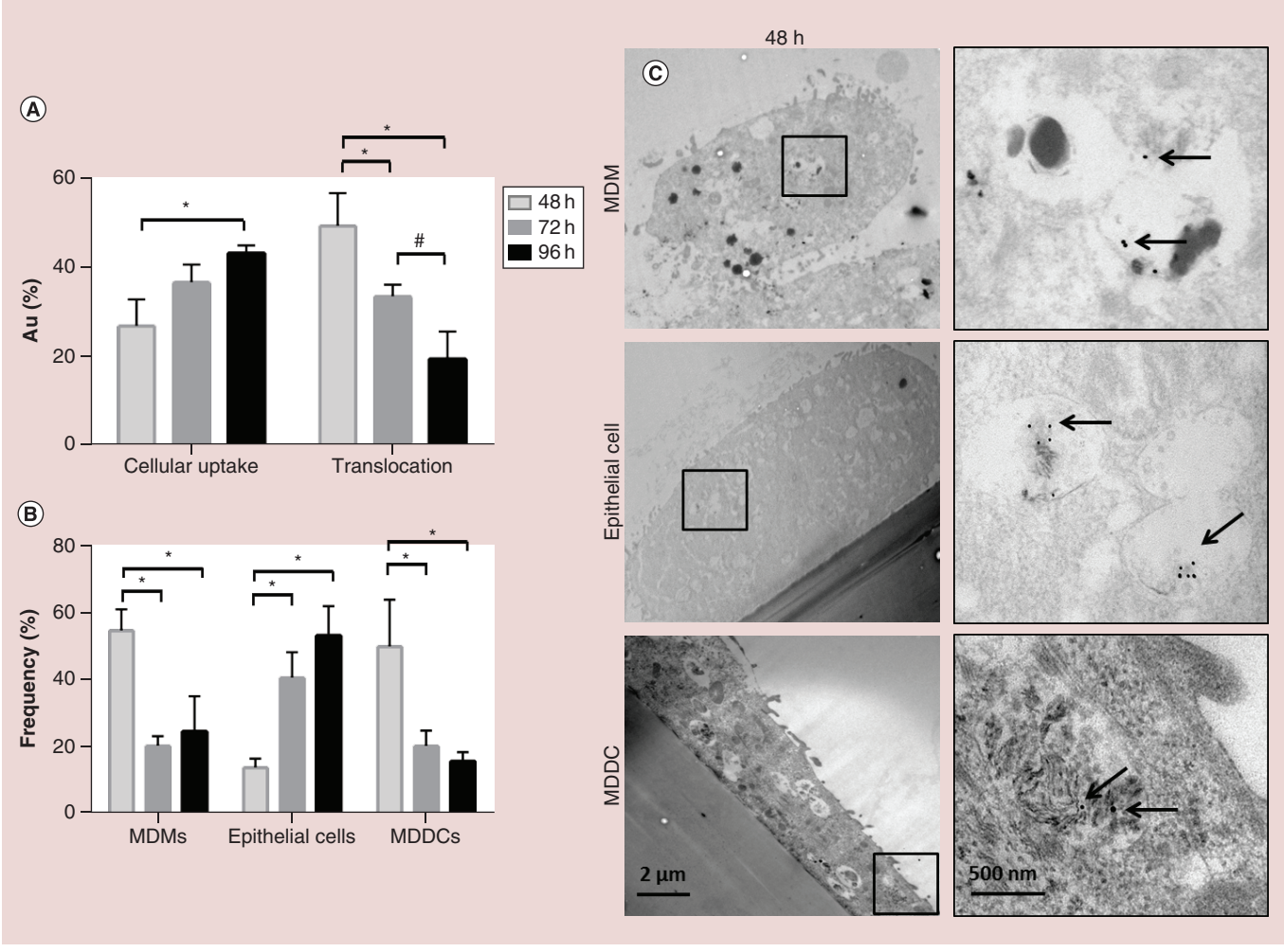

Figure 3. Interaction of Au nanoparticles with the co-culture model of the human lung epithelial tissue barrier following short-term repeated aerosol exposure. (A) Percentage of Au in the cellular and translocated fraction as measured by the inductively coupled plasma atomic emission spectroscopy (ICP-OES). **(B)** Au nanoparticle association within the different cell types of the *in vitro* model (flow cytometry analysis). **(C)** Transmission electron microscopy images show the presence of internalized Au nanoparticles at the different cell types of the co-culture model, following single aerosol exposure (48 h). Black arrows point out the position of the particles.
*$p < 0.05$.
MDDC: Monocyte-derived dendritic cell; MDM: Monocyte-derived macrophage.

Integrity of the alveolar epithelial monolayer

The integrity of the alveolar epithelium in the triple cell co-culture, following repeated AuNPs aerosolization, was evaluated by assessing the permeability of Dextran Blue. As shown in Supplementary Figure 5A, no effect was observed for Dextran Blue translocation in AuNPs-exposed cells compared with untreated cultures at any of the tested time points. Consistent with the latter observation, laser scanning confocal microscope images confirmed that the cellular morphology and the epithelial monolayer structure were not impaired upon repeated exposure to AuNPs (Supplementary Figure 5B). Those findings therefore support the hypothesis that the observed MDDC uptake and translocation to the basolateral side can be attributed to the interaction within the cells and not to decreased integrity of the epithelial monolayer.

Cellular response

Cytotoxicity/apoptosis

Assessment of the LDH activity in the supernatant of exposed cells did not show cytotoxic reactions in cultures exposed repeatedly for up to 96 h to aerosolized AuNPs when compared with control (Figure 4A).

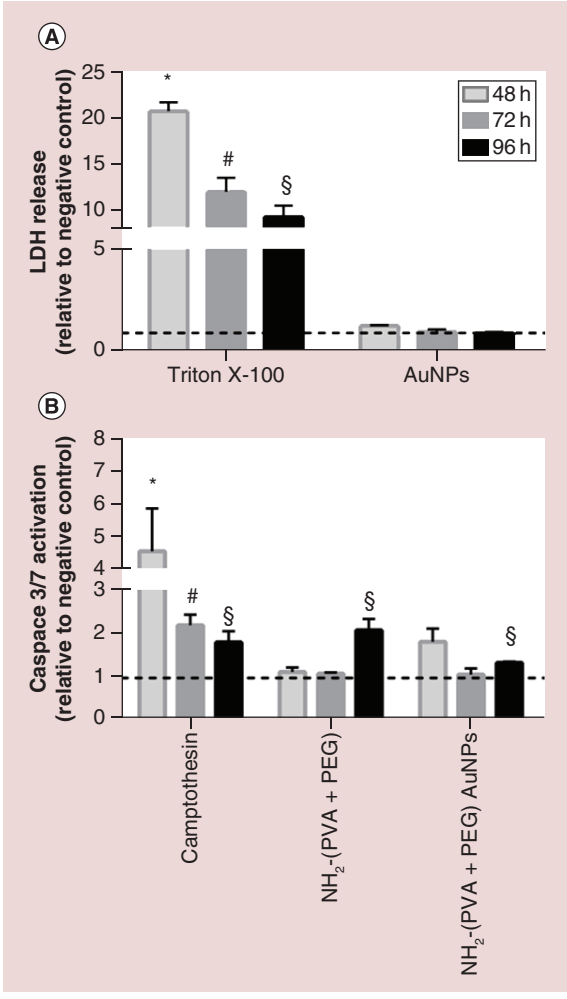

Figure 4. Cytotoxicity and apoptosis. (A) LDH release and **(B)** activation of caspase 3 and 7 in the human model of the alveolar epithelial tissue barrier, following repeated exposure to functionalized Au nanoparticles for up to 96 h. Dashed lines (- - -) represent the level of the negative control. Values were considered significant compared with the negative control when $p < 0.05$ (* for 48 h, # for 72 h and § for the 96 h time point). Co-cultures exposed apically to Triton X-100 (0.2%) and camptothecin (2 μm) were used as positive controls for the cytotoxicity and apoptosis determination, respectively.

To address the potential of surface-modified AuNPs to cause apoptotic effects upon repeated administration, the activation of caspase 3 and 7 in the cellular system was assessed. Elevated caspase activation was observed in the co-cultures, following single AuNP aerosolization at 48-h time point; however, this was not statistically significant ($p < 0.05$). Notably, significant apoptosis was reported for the AuNPs-exposed cultures at 96-h time point, compared with the negative control as shown from the caspase 3/7 activity (Figure 4B). Detailed investigation of the observed apoptotic events using the Annexin V assay further confirmed the findings of the caspase response. More specifically, cell cultures exposed repeatedly for three-times to aerosolized AuNPs (96 h) revealed a significant reduction in the amount of healthy cells, followed by a significant increase of the early and late apoptotic cells (Supplementary Figure 6A). Signs of apoptosis were also visualized by nuclear staining in AuNP-treated cells at the 96-h time point (Supplementary Figure 6B). To examine if the surface modification itself is responsible for the observed apoptotic effects, control cultures exposed to the (PVA/PEG)-NH_2 polymer alone, were also analyzed. No increase in apoptotic events were shown after single or two repeated polymer aerosolizations in the cultures; however, the third administration did induce significant activation of caspase 3 and 7 as well as significant increase in early apoptotic events at 96-h timeframe.

Proinflammatory response

Short-term exposure to aerosolized AuNPs did not cause any effect in the secretion of the critical proinflammatory markers IL-1β, TNF-α and IL-8, indicating that the tested AuNPs did not trigger proinflammatory responses in the presented cellular system after repeated administration (Figure 5).

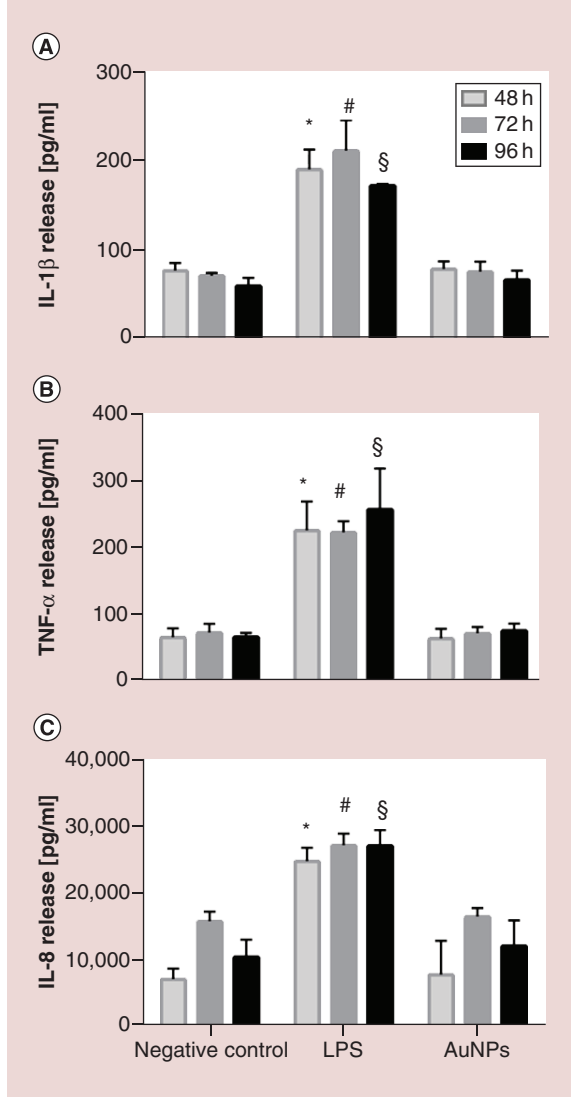

Figure 5. Release of proinflammatory mediators. (A) IL-1β, **(B)** TNF-α and **(C)** IL-8 secretion after short-term repeated exposures NH_2-(polyvinyl alcohol/PEG) Au nanoparticles. Values were considered significant compared with the negative control when $p < 0.05$ (* for 48 h, # for 72 h and § for the 96-h time point). Lipopolysaccharide (1 μg/ml) was added to the cultures for 24 h as a positive control for proinflammatory responses.

Discussion

Recently, we have established a library of fluorescence-encoded AuNPs in order to investigate how surface modification can modulate the NP–cell interaction and in particular the internalization by primary dendritic cells [17,18]. This particle library contained groups of differently charged homo- and hetero-functional labeled or unlabeled AuNPs using PVA and PEG-based polymers for particle coating and stabilization. Heterofunctional fluorescently labeled (PVA/PEG)-NH_2 AuNPs were selected for the present study, since these particles showed a high degree of cellular internalization and substantial cell viability (even at high doses of 100 μg/ml) after 16 h submerged exposure to MDDCs [17]. Therefore, this specific AuNPs type is ideal for studying the interaction within the different cells types of an advanced lung model after short-term repeated administration. Moreover, the utilization of fluorescently labeled NPs allows the detection of fluorescence positive cells by flow cytometry [34].

The synthesized AuNPs were fully characterized before and after the aerosolization process using various methods, that is, UV-Vis, DLS, ζ-potential and TEM. The stability of the AuNPs was confirmed by UV-Vis analysis as no signs of aggregation or shifting of the spectra were observed neither before nor after the aerosolization experiments. Although AuNPs were functionalized with positive functional groups, a slightly negative ζ-potential was observed which can be connected with the reduced number of protonated amino groups at neutral pH or the remaining strongly negative citrate ions [17,30]. Notably, the hydrodynamic diameter of the aerosolized particles remains similar to the hydrodynamic diameter of the stock suspension, therefore, confirming that the aerosolization process did not impair the surface polymer coating. Thorough NP characterization prior to as well as following the aerosol

exposures is crucial to verify that NPs maintain their characteristics and to obtain reliable data, which truly reflects their properties when they come in contact with biological systems.

Evaluation of the AuNP uptake and possible translocation across the epithelial barrier using ICP-OES, demonstrated a significant enhanced internalization of particles in the co-culture model following repeated AuNP administration from 48 (single exposure) to 96 h (three repeated exposures), thus particle accumulation in the cells was reinforced through repeated NP treatment. On the other hand, NP translocation showed a contradictory pattern. Single AuNP administration resulted in the highest translocation levels which were then significantly reduced at latter time points.

To ensure that the obtained translocation findings truly reflect the fate of internalized NP when cross the alveolar epithelium in the co-culture system and do not originate from alterations of its integrity, the integrity of the epithelial barrier was also examined by evaluating the permeability to dextran, a common approach to assess the permeability of epithelial barriers [35,36]. The epithelium of AuNP repeatedly exposed cultures formed a tight and confluent monolayer conformation at all tested time points, which can be further verified by the illustrated morphological images. It is therefore evident that the observed NP translocation cannot occur from the impairment of the epithelial structure.

Contrary to our findings, Durantie *et al.* have observed lower rates (3–10%) of PVA/polyallyl amine-coated AuNPs translocated in the basolateral side after single/acute NPs administration using the Vitrocell® (Vitrocell Systems, Waldkirch, Germany) Cloud system in the same multicellular lung model [37]. The difference in the translocated fraction can be attributed to the different NP coating, exposure system as well as deposited doses applied.

In a recent *in vivo* study, a size- and surface charge-dependent translocation of radiolabeled AuNPs was shown after single intratracheal instillation. In particular, it has been observed that particle translocation inversely depends on particle size and that negatively charged AuNPs show higher degree of translocation compared with their positive-charged counterparts. The percentage of translocated particles following post exposure 24 h was in the range of 0.5–10%, depending on the Au core size, that is, increasing with decreasing core size [38]. In a related study, the percentage of translocated AuNPs in the blood in just 2 h after single-dose inhalation was approximately 1.2% which was claimed as relative high, considering the complexity of the respiratory tract and the early timeframe tested [39].

While our translocation rates are significantly higher than that obtained in these animal studies it should be noted that our *in vitro* model although highly advanced and closer to the human lung physiology compared with other existing cellular models, is not as complex as the real *in vivo* air–blood barrier. Under *in vivo* conditions, particles translocated through the alveolar epithelial layer, also need to pass over the interstitium and subsequently cross the vascular endothelial layer to reach the bloodstream [40]. It has been demonstrated that a significant amount of translocated NPs might be isolated in the interstitium or be transported by phagocytic cells to the lymph nodes through the lymphatic drainage system [41]. Therefore, the absence of this clearance mechanism in our model might have a significant influence in the fraction of translocated particles. *In vivo* particle translocation to the bloodstream was also reported following exposure to different NP types, that is, polystyrene, fullerene [42,43]. Increased translocation of potential biomedical NPs is an important feature that can be further applied for nanocarrier-based drug delivery to the systemic circulation. Inhaled insulin particles have been already developed for diabetes treatment and their effective delivery is based on efficient pulmonary translocation [44].

To investigate the distribution of AuNPs within the different cell types of the co-culture model upon repeated administration a novel flow cytometry-based approach was applied [28]. By using cell markers specific for the cell types present in the co-culture, we could determine information on the NP interaction with the three cell types. An important defense feature of the respiratory tract is the phagocytic activity of macrophages which prevents potential proinflammatory effects by sufficient clearance of inhaled pathogens, particles and cellular debris, thus preserving the regular homeostasis of the epithelial tissue and the vital functionality of the alveolar gas exchange [45]. The presented flow cytometry data indicated that the majority of AuNPs were internalized by macrophages. The key role of macrophages in both pro- and anti-inflammatory events in response to different signals has been highlighted in several reports [46]. In addition, Brandenberger *et al.* first demonstrated the capacity of A549 epithelial cells to internalize citrate-stabilized AuNPs after single ALICE exposure in the same *in vitro* system [26]. In the present study repeated AuNPs aerosol exposures resulted in increased particle accumulation over the days of exposure in epithelial cells, possibly due to macrophage saturation. The interaction of AuNPs with the MDMs and epithelial cells was further confirmed by TEM images captured at the different tested time points.

Of note, flow cytometry analysis revealed that the MDDCs located on the basal side showed a high degree of interaction with the AuNPs after single aerosolization (48 h). However, this increased uptake was followed by a significant reduction at later tested time points (72 and 96 h). Most importantly, the uptake pattern of dendritic cells matched exactly the obtained translocation pattern, hence confirmed the translocation results. The translocation through the transwell membrane was additionally confirmed by TEM imaging. More specifically, AuNPs were identified in MDDCs at all tested time points. It has been hypothesized that NPs can cross the epithelial layer in the co-culture model by two mechanisms: either MDMs can directly deliver internalized NPs to MDDCs located in basal side; or the MDDCs can collect the particles by extending processes to the epithelial side through the insert pores and the tight junctions [25]. Indeed, we were able to visualize AuNPs while translocating via the insert pores to the basolateral MDDCs side through cell to cell interactions. Moreover, in the basolateral side particles were captured in cellular protrusions. Therefore, the obtained TEM images further support the ICP-OES and flow cytometry results.

Antigen-presenting cells and more specifically MDDCs have been proposed as an ideal target for novel nanocarrier-based drug delivery approaches [47,48]. In our recent publication, we have provided evidence that DC-SIGN conjugation to AuNPs resulted in elevated MDDC targeting and activation in the same co-culture model [27]. Therefore, considering the high degree of particles taken up by the MDDCs in the present study, the applied AuNPs could have the potential for biomedical-specific cell targeting applications following conjugation with the appropriate antigen.

Repeated AuNP exposure did not show any signs of cytotoxicity; however, significant cell apoptosis was observed at the 96-h time point as shown from the caspase 3/7 activity. Activation of caspase 3 and 7 is a clear sign of early apoptotic events, which eventually leads to protein cleavage and subsequently cell disassembly [49]. Caspase activation is a fundamental process for the development of a complete apoptotic phenotype; however, as apoptosis is a complex mechanism that cannot be defined by a single parameter we also evaluated Annexin V, another well-known apoptotic marker. Annexin V cell analysis confirmed the findings reported by caspase evaluation, resulting in a significant increase in the percentage of early and late apoptotic cells after repeated AuNP exposures at 96-h time point. In a recent publication, significant late apoptosis was induced in the same co-culture model after single aerosol administration to PVA-NH_2 AuNPs [27], suggesting a possible role of the surface polymer in the induction of apoptosis. Therefore, we also exposed the cells to the (PVA/PEG)-NH_2 polymer only, in order to determine if the polymer is responsible for the enhanced apoptotic levels observed. Indeed, significant elevated apoptosis was demonstrated in both end points in polymer-only exposed cultures after repeated aerosolization at 96 h. Ruenraroengsak *et al.* also reported substantial apoptosis accompanied by severe cell damage and holes on the cell membrane on alveolar type I immortalized cells following 24-h suspension exposure to amine-modified polystyrene NPs which were attributed to the surface modification [50]. Biological effects caused by aminated surface were also shown in another recent study where iron-oxide and silicon-oxide NPs caused substantial cell death and IL-8 response in A549 monocultures [51]. On the contrary, Strehl *et al.* although reported a dose-dependent cytokine release in blood-derived monocytes and MDMs following exposure to aminated-PVA superparamagnetic iron-oxide NPs, the cell survival and proliferation was increased [52]. However, the absence of cytotoxic reactions or morphological alterations and the intact membrane integrity confirmed by the permeability tests, indicates that the observed apoptosis in the present study have a relative minor influence on the overall viability and functionality of the co-culture model at the tested conditions.

The proinflammatory response upon repeated AuNPs exposures was addressed by measuring the secretion of the crucial proinflammatory mediators IL1-β, TNF-α and IL-8, involved in the pathogenesis and exacerbation of lung diseases, through the inflammasome activation pathway and various proinflammatory pathways [53–55]. Therefore, their evaluation clearly signifies the inflammatory response of the *in vitro* system under the presented test conditions. Our findings demonstrated that short-term-repeated AuNPs exposures did not elicit any effect in the cytokine secretion, suggesting that repeated AuNPs aerosolization did not induce proinflammatory activity. In line with our observations no proinflammatory reactions were reported after single aerosolization of either negative or positive surface-charged PVA-AuNPs at the same cellular model [27]. Similarly, Brandenberger *et al.* showed that 15 nm citrate AuNPs did not upregulate TNF-α and IL-8 expression in the triple cell co-culture upon single exposure [26].

Conclusion

By applying an innovative flow cytometry approach combined with TEM visualization and ICP-OES analysis it was possible to determine the biological impact, interaction and translocation of AuNPs functionalized with a (PVA/PEG)-NH_2 polymer within the different cell types of a complex *in vitro* human lung epithelial tissue barrier model at realistic conditions resembling their inhalation upon single and repeated aerosol administration. Our results revealed increased particle accumulation in both macrophages and epithelial cells following repeated short-term exposure. Most importantly, MDDCs showed elevated levels of particle internalization making them an interesting target for potential future biomedical applications. Although repeated NP administration over 3 days did not have any effect in cytotoxicity, morphology or cytokine release, increased apoptosis was observed with only mild effect in overall cellular response, the response could; however, be attributed to the (PVA/PEG)-NH_2 polymer. In conclusion, our results suggest that repeated exposures of biomedical AuNPs have to be studied in more details in both *in vitro* and *in vivo* systems.

Summary points

- The distribution and impact of aerosol-delivered functionalized AuNPs upon repeated administration were explored in a complex *in vitro* human lung epithelial tissue barrier model applying an air–liquid interface exposure approach.
- By applying an innovative flow cytometry approach combined with transmission electron microscopy visualization and ICP-OES analysis the interaction and translocation of (polyvinyl alcohol/PEG)-NH2 Au nanoparticles (NPs) were determined within the different cell types of the 3D lung model upon single and short-term-repeated aerosol administration.
- Repeated AuNP aerosolization resulted in NP accumulation in macrophages and epithelial cells.
- Dendritic cells demonstrated substantial NP internalization after single administration which was reduced at later time points.
- Repeated AuNP administration over 3 days did not have any effect in cytotoxicity, morphology or cytokine release.
- Increased apoptosis was observed at 96 h with only mild effect in overall cellular response.
- Apoptosis was attributed to the (polyvinyl alcohol/PEG)-NH_2 polymer.
- These results indicate the importance of repeated exposures in addressing potential effects of biomedical NPs.

Supplementary data

To view the supplementary data that accompany this paper please visit the journal website at: www.futuremedicine.com/doi/suppl/10.2217/nnm-2017-0358

Financial & competing interests disclosure

This study was supported by the Swiss National Science Foundation (Grant Nr. 310030_159847/1) and the Adolphe Merkle Foundation. The authors have no other relevant affiliations or financial involvement with any organization or entity with a financial interest in or financial conflict with the subject matter or materials discussed in the manuscript apart from those disclosed.

No writing assistance was utilized in the production of this manuscript.

Ethical conduct of research

The authors state that they have obtained appropriate institutional review board approval or have followed the principles outlined in the Declaration of Helsinki for all human or animal experimental investigations. In addition, for investigations involving human subjects, informed consent has been obtained from the participants involved.

References

Papers of special note have been highlighted as: • of interest; •• of considerable interest

1. Weibel ER. Principles and methods for the morphometric study of the lung and other organs. *Lab. Invest.* 12, 131–155 (1963).
2. Gehr P, Bachofen M, Weibel ER. The normal human lung: ultrastructure and morphometric estimation of diffusion capacity. *Respir. Physiol.* 32, 121–140 (1978).
3. Nicod LP. Lung defenses: an overview. *Eur. Respir. Rev.* 95, 45–50 (2005).
4. Patton JS, Fishburn C, Weers JG. The lungs as a portal of entry for systemic drug delivery. *Proc. Am. Thorac. Soc.* 1, 338–344 (2004).
5. Müller L, Andrea L, Johnston BD *et al.* Inhalation pathway as a promising portal of entry: what has to be considered in designing new nanomaterials for biomedical application? In: *Handbook of Nanotoxicology, Nanomedicine And Stem Cell Use In Toxicology.* Sahu SC, Casciano D (Eds). John Wiley & Sons Ltd, NJ, USA (2014).
6. Patton JS, Byron P. Inhaling medicines: delivering drugs to the body through the lungs. *Nat. Rev. Drug Discov.* 6, 67–74 (2007).

•• **Provides an in-depth discussion of the advantages of the physiological features of the lung for medical applications, such as systemic delivery of therapeutics via inhalation.**

7. Laube BL, Janssens H, De Jongh FH *et al.* What the pulmonary specialist should know about the new inhalation therapies. *Eur. Respir. J.* 37(6), 1308–1331 (2011).
8. Csaba N, Garcia-Fuentes M, Alonso MJ. Nanoparticles for nasal vaccination. *Adv. Drug Deliv. Rev.* 61(2), 140–157 (2009).
9. Seydoux E, Rodriguez-Lorenzo L, Blom RA *et al.* Pulmonary delivery of cationic gold nanoparticles boost antigen-specific $CD4^+$ T cell proliferation. *Nanomedicine* 12, 1815–1826 (2016).
10. Fytianos K, Drasler B, Blank F *et al.* Current *in vitro* approaches to assess nanoparticle interactions with lung cells. *Nanomedicine (Lond.)* 11(18), 2457–2469 (2016).
11. Doane TL, Burda C. The unique role of nanoparticles in nanomedicine: imaging, drug delivery and therapy. *Chem. Soc. Rev.* 41(7), 2885–2911 (2012).
12. Thorley AJ, Tetley T. New perspectives in nanomedicine. *Pharmacol. Ther.* 176–185 (140), 2 (2013).
13. Oberdorster G, Maynard A, Donaldson K, Castranova V, Fitzpatrick J, Ausman K. Principles for characterizing the potential human health effects from exposure to nanomaterials: elements of a screening strategy. *Part. Fibre Toxicol.* 2, 8 (2005).
14. Bachler G, Losert S, Umehara Y, Von Goetz N *et al.* Translocation of gold nanoparticles across the lung epithelial tissue barrier: combining *in vitro* and *in silico* methods to substitute *in vivo* experiments. *Part. Fibre Toxicol.* 12, 18 (2015).
15. Dreaden EC, Alkilany A, Huang X, Murphy CJ, El-Sayed MA. The golden age: gold nanoparticles for biomedicine. *Chem. Soc. Rev.* 41, 2740–2779 (2012).
16. Dykman L, Nikolai K. Gold nanoparticles in biomedical applications: recent advances and perspectives. *Chem. Soc. Rev.* 2012(41), 2256–2282 (2012).
17. Rodriguez-Lorenzo L, Fytianos K, Blank F, Von Garnier C, Rothen-Rutishauser B, Petri-Fink A. Fluorescence-encoded gold nanoparticles: library design and modulation of cellular uptake into dendritic cells. *Small* 10(7), 1341–1350 (2014).
18. Fytianos K, Rodriguez-Lorenzo L, Clift MJD *et al.* Uptake efficiency of surface modified gold nanoparticles does not correlate with functional changes and cytokine secretion in human dendritic cells *in vitro*. *Nanomedicine (Lond.)* 11, 633–644 (2015).
19. Lasagna-Reeves C, Gonzalez-Romero D, Barria MA *et al.* Bioaccumulation and toxicity of gold nanoparticles after repeated administration in mice. *Biochem. Biophysl. Res. Com.* 393, 649–655 (2010).
20. Lenz AG, Karg E, Lentner B, Dittrich V, Brandenberger C, Rothen-Rutishauser B. A dose-controlled system for air–liquid interface cell exposure and application to zinc oxide nanoparticles. *Part Fibre Toxicol.* 6, 32 (2009).

• **Describes an air–liquid interface cell exposure system to assess the effects of aerosolized nanoparticles.**

21. Rothen-Rutishauser BM, Kiama S, Gehr P. A three-dimensional cellular model of the human respiratory tract to study the interaction with particles. *Am. J. Respir. Cell Mol. Biol.* 32(4), 281–289 (2005).

• **Description and characterization of the 3D lung system, as represented by epithelial cells, macrophages and dendritic cells, suitable for investigation of particle interactions with lung immune cells.**

22. Chortarea S, Clift MJD, Vanhecke D *et al.* Repeated exposure to carbon nanotube-based aerosols does not affect the functional properties of a 3D human epithelial airway model. *Nanotoxicology* 9, 983–993 (2015).
23. Enustun BV, Turkevich J. Coagulation of colloidal gold. *J. Am. Chem. Soc.* 85(21), 3317–3328 (1963).
24. Blank F, Gerber P, Rothen-Rutishauser B, Sakulkhu U, Salaklang J, De Peyer K. Biomedical nanoparticles modulate specific $CD4^+$ T cell stimulation by inhibition of antigen processing in dendritic cells. *Nanotoxicology* 5(4), 606–621 (2011).
25. Blank F, Rothen-Rutishauser B, Gehr P. Dendritic cells and macrophages form a transepithelial network against foreign particulate antigens. *Am. J. Respir. Cell Mol. Biol.* 36, 669–677 (2007).
26. Brandenberger C, R-R B, Muhlfeld C, Schmid O, Ferron GA, Maier KL. Effects and uptake of gold nanoparticles deposited at the air–liquid interface of a human epithelial airway model. *Toxicol. Appl. Pharmacol.* 242, 56–65 (2009).

27. Fytianos K, Chortarea S, Rodriguez-Lorenzo L *et al*. Aerosol delivery of functionalized gold nanoparticles target and activate dendritic cells in a 3D lung cellular model. *ACS Nano* 11(1), 375–383 (2017).
28. Clift MJD, Fytianos K, Vanhecke D, Hočevar S, Petri-Fink A, Rothen-Rutishauser B. A novel technique to determine the cell type specific response within an *in vitro* co-culture model via multi color flow cytometry. *Sci. Rep*. 7(1), 234 (2017).
29. Mahida YR, Makh S, Hyde S, Gray T, Borriello SP. Effect of clostridium difficile toxin a on human intestinal epithelial cells: induction of interleukin 8 production and apoptosis after cell detachment. *Gut* 38, 337–347 (1996).
30. Zhang Y, Pan H, Zhang P *et al.* Functionalized quantum dots induce proinflammatory responses *in vitro*: the role of terminal functional group-associated endocytic pathways. *Nanoscale* 5(13), 5919–5929 (2013).
31. Brandenberger C, Mühlfeld C, Ali Z, Lenz AG *et al.* Quantitative evaluation of cellular uptake and trafficking of plain and polyethylene glycol-coated gold nanoparticles. *Small* 6, 1669–1678 (2010).
32. Herzog F, Clift M, Piccapietra F *et al*. Exposure of silver-nanoparticles and silver-ions to lung cells *in vitro* at the air–liquid interface. *Part. Fibre Toxicol.* 10, 11 (2013).
33. Chortarea S, Barosova H, Clift MJD, Wick P, Petri-Fink A, Rothen-Rutishauser B. Human asthmatic bronchial cells are more susceptible to sub-chronic repeated exposures of aerosolized carbon nanotubes at occupationally-relevant doses. *ACS Nano* 11(8), 7615–7625 (2017).
34. Vanhecke D, Rodriguez-Lorenzo L, Clift MJD, Blank F, Fink-Petri A, Rothen-Rutishauser B. Quantification of nanoparticles at the single cell level – an overview about state-of-the art techniques and their limitations. *Nanomedicine (Lond.)* 9, 1885–1900 (2014).
35. Bouwmeester H, Poortman J, Peters RJ *et al.* Characterization of translocation of silver nanoparticles and effects on whole-genome gene expression using an *in vitro* intestinal epithelium coculture model. *ACS Nano* 24(5), 4091–4103 (2011).
36. Elbert KJ, Schäfer U, Schäfers HJ, Kim KJ, Lee VH, Lehr CM. Monolayers of human alveolar epithelial cells in primary culture for pulmonary absorption and transport studies. *Pharm. Res.* 16(5), 601–608 (1999).
37. Durantie E, Vanhecke D, Rodriguez-Lorenzo L *et al.* Biokinetics of single and aggregated gold nanoparticles exposed to the human lung epithelial tissue barrier at the air–liquid interface. *Part. Fibre Toxicol.* 14, 49 (2017).
38. Kreyling WG, Hirn S, Möller W *et al.* Air–blood barrier translocation of tracheally instilled gold nanoparticles inversely depends on particle size. *ACS Nano* 8(1), 222–233 (2013).

•• **An *in vivo* study that reports that the translocation of gold nanoparticles across the air–blood barrier, intratracheally instilled into rats, depends on the nanoparticle surface charge and specific surface area.**

39. Schleh C, Holzwarth U, Hirn S *et al*. Biodistribution of inhaled gold nanoparticles in mice and the influence of surfactant protein D. *J. Aerosol Med. Pulm. Drug Deliv.* 26(1), 24–30 (2013).
40. Ochs MW. Functional design of the human lung for gas exchange. In: *Fishman's Pulmonary Diseases And Disorders.* McGraw–Hill Medical, NY, USA (2007).
41. Porter DW, Wu N, Hubbs AF *et al.* Differential mouse pulmonary dose and time course responses to titanium dioxide nanospheres and nanobelts. *Toxicol. Sci.* 131(1), 179–193 (2013).
42. Sarlo K, Blackburn K, Clark ED *et al.* Tissue distribution of 20 nm, 100 nm and 1000 nm fluorescent polystyrene latex nanospheres following acute systemic or acute and repeat airway exposure in the rat. *Toxicology* 263, 117–126 (2009).
43. Naota M, Shimada A, Morita T, Inoue K, Takano H. Translocation pathway of the intratracheally instilled C60 fullerene from the lung into the blood circulation in the mouse: possible association of diffusion and caveolae mediated pinocytosis. *Toxicol. Pathol.* 37, 456–462 (2009).
44. Bi R, Shao W, Wang Q, Zhang N. Solid lipid nanoparticles as insulin inhalation carriers for enhanced pulmonary delivery. *J. Biomed. Nanotechnol.* 5(1), 84–92 (2009).
45. Kirby AC, Coles M, Kaye PM. Alveolar macrophages transport pathogens to lung draining lymph nodes. *J. Immunol.* 183(3), 1983–1989 (2009).
46. Mosser DM, Edwards J. Exploring the full spectrum of macrophage activation. *Nat. Rev. Immunol.* 8(12), 958–969 (2008).
47. Joshi MD, Unger W, Storm G, Van Kooyk Y, Mastrobattista E. Targeting tumor antigens to dendritic cells using particulate carriers. *J. Control. Rel.* 161(1), 25–37 (2012).
48. Kunda NF, Somavarapu S, Gordon SB, Hutcheon GA, Saleem IY. Nanocarriers targeting dendritic cells for pulmonary vaccine delivery. *Pharm. Res.* 30(2), 325–341 (2013).
49. Slee EA, Adrain C, Martin SJ. Serial killers: ordering caspase activation events in apoptosis. *Cell Death Differ.* 6(11), 1067–1074 (1999).
50. Ruenraroengsak P, Novak P, Berhanu D *et al.* Respiratory epithelial cytotoxicity and membrane damage (holes) caused by amine-modified nanoparticles. *Nanotoxicology* 6(1), 94–108 (2012).
51. Choi SJ, Oh J, Choy JH. Toxicological effects of inorganic nanoparticles on human lung cancer A549 cells which was directly related to the positive surface charge. *J. Inorg. Biochem.* 103(3), 463–471 (2009).
52. Strehl C, Gaber T, Maurizi L *et al.* Effects of PVA coated nanoparticles on human immune cells. *Int. J. Nanomedicine* 8(10), 3429–3445 (2015).

53. Dinarello CA. Biologic basis for inteleukin 1 in disease. *Blood* 87(6), 2095–2147 (1996).

54. Mukhopadhyay S, Hoidal J, Mukherjee T. Role of TNFα in pulmonary pathophysiology. *Respir. Res.* 7, 125 (2006).

55. Groth A, Vrugt B, Brock M, Speich R, Ulrich S, Huber LC. Inflammatory cytokines in pulmonary hypertension. *Respir. Res.* 16(15), 47 (2014).